Correlation of permeability values with flow channel diameters determined by 3D-image analysis of a woven textile

G. Rieber [1], O. Wirjadi [2] and P. Mitschang [1]

[1] *Institut für Verbundwerkstoffe, Erwin-Schrödinger-Str. Geb. 58, D-67663 Kaiserslautern, Germany:* gunnar.rieber@ivw.uni-kl.de

[2] *Fraunhofer-Institut für Techno- und Wirtschaftsmathematik, Fraunhofer-Platz 1, D-67663 Kaiserslautern, Germany:* oliver.wirjadi@itwm.fraunhofer.de

ABSTRACT: Attempts to model and to better understand permeability by studying the build-up of textiles are widespread [1-3]. Yet, textile structure data are rarely based on quantitative analysis of high resolution 3D-images of the composite structure at multiple fiber volume fractions.
Within the present study, micro-computer tomography (µCT) images of glass twill weave reinforced epoxy are analyzed. After subtracting the fibers from the images, the geometry of the matrix space, below-named pore space, is analyzed by a process called spherical granulometry. It was possible to directly calculate the permeability with theses pore diameters using a combination of the Darcy and Hagen-Poiseuille formulae: the permeability value K is proportional to the squared diameter $(d^2/96)$ of the flow channel. As permeability-dominating pore diameters the 10 %-, 25 %- and 40 %-quantiles of the cumulative pore volume have been determined for fiber volume fractions from 40 % to 56 %. The calculated results are in accordance with global permeability values determined by 2D and 3D permeability measurements.

INTRODUCTION

For robust infusion and injection processes, the permeability should be known. Currently, the most reliable and commonly used way to determine permeability values is via experimental measurements. For two decades, several groups have been working intensively on modeling the permeability of yarns and textiles. This furthers the understanding of the principle relationships between textile structures and their permeabilities. This can reduce laborious experimental characterization work.
3D images of composites have rarely been used to determine the geometry of fibrous preforms and its change with increasing fiber volume fractions [4]. Published 3D textile structures [5-8] are therefore partly based on assumptions. To overcome the inability to accurately determine the detailed geometry of the fibrous preform, Dunkers et al. acquired optical coherence tomography (OCT) images of a sample with a fiber volume

fraction of 44 % and unidirectional fiber orientation. These 3D images (2 x 1.9 x 7 mm³) were processed to binary images and input into a 3D Lattice Boltzman flow code. Axial and transverse permeability values were determined. The influence of image processing was shown, and agreement with experimental results was quite good.

The present study was driven by a similar motivation: The goal is to quantitatively analyze the pore-size distribution (i.e. the space) between the fibers and to correlate these geometrical parameters based on 3D images of a composite laminate with global permeability values at different fiber volume fractions. The analyzed composite consisted of 5, 6 and 7 layers of a twill weave textile. The 3D images have been generated by micro computer tomography (µCT). The µCT data has a spatial resolution of 2 µm for small samples, in comparison to OCT images with a resolution of 15 – 30 µm. The images were then quantitatively analyzed using the MAVI image processing software developed by the Fraunhofer-Institute for Industrial Mathematics ITWM, which has previously been used to solve similar problems, cf. e.g. [9, 10]. This software enables quantitative 3D analysis of complex geometries. The permeability values are obtained from unsaturated in-plane radial flow and through-the-thickness experimental measurements. Permeability-determining quantiles of the pore-size distribution that fit best to the experimental data for each fiber volume fraction are suggested. The 10%-quantile for a fiber volume fraction of 56 % is in accordance with Hazen [11, 12], who as well suggested that smaller particles or pores of a porous structure determine its permeability. To regard interconnected capillaries as a series of parallel streamlines was validated by Williams [13]. This study is an attempt to link the microstructure of the porous material with the observed flow behavior.

MATERIALS & METHODS

The reinforcement textile used for this study is a glass fiber twill weave textile (390 g/m²) equipped with a finish for epoxy resin (K 506). The textile is built up anisotropically: the linear density in weft direction is 272 tex with 6.7 yarns (picks) per cm, the linear density in warp direction is 68 tex x 5 t0 (multiple wound yarn) with 6.0 yarns (picks) per cm (Schloesser & Cramer, art. no. 3106).

These textile layers (465 x 465 mm) have been injected by epoxy resin to produce a composite suitable for µCT analysis. To achieve three different fiber volume fractions, 5, 6 and 7 textile layers have been placed inside a 2 mm cavity of the RTM mold. Out of these composite sheets, three smaller samples have been cut using a diamond saw, each with sufficient dimensions for the textile to be well represented (5 x 5 x 2 mm).

The in-plane permeability was determined by a radial flow experiment as described in [14, 15]. The permeability algorithm is based on the one developed by Douglas et al. and Adams et al.. The through-the-thickness permeability was determined by an ultrasound time of flight measurement described in [16]. Both measurements were unsaturated.

The µCT images were generated with the voltage set to 100kV and the current set to 90µA. Using the gray values of the glass fibers in the image data, the fibers have been subtracted from the 3D image such that only the matrix structure (resin) was left (Fig. 2, right). In order to reduce effects caused by noise and limited resolution, only those matrix areas larger than the fiber diameter (9 µm) have been taken into account for the

image analysis. Fan et al. specify the size of microscale gaps from 50 nm to 5 µm [17]. Therefore microscale flow is neglected in this study.

To characterize this matrix structure, the spherical granulometry distribution known from mathematical morphology [18] has been used: Consider the set of points attributed to the pore space in an image, which has been determined using smoothing filters and image binarization. That pore space (in the present case: the <u>matrix </u>structure) is digitally closed using a ball with increasing diameter. By applying this sequence of so-called closure operations, one removes the pores (matrix space between the fibers) from an image, starting with small pores until no porosity will be left in the data. When using a three dimensional sphere (i.e., a ball B(d) with diameter d) as in the present case, one measures the spherical granulometry distribution function by recording the volume fraction of the pore space that disappears during each of these sequential closure operations. The result are cumulative distribution functions of relative pore space volume over the local pore space diameter d as shown in Fig. 2. An alternative interpretation of the spherical granulometry is as follows. For each point x in the pore space, attribute x to the largest ball B(d) that can be fit into the pore space and which covers x. By computing the histogram of points x covered by all balls of diameter d from 0 to the maximal pore space diameter, one will again end up with the spherical granulometry.

RESULTS

In figure 1, the results of the permeability measurement results are presented. The K1 and K2 values have been determined by a radial flow permeability measurement. The K3 values have been generated by an ultrasound through-the-thickness measurement. The global permeability curve is an exponential regression line of the third root of K1*K2*K3.
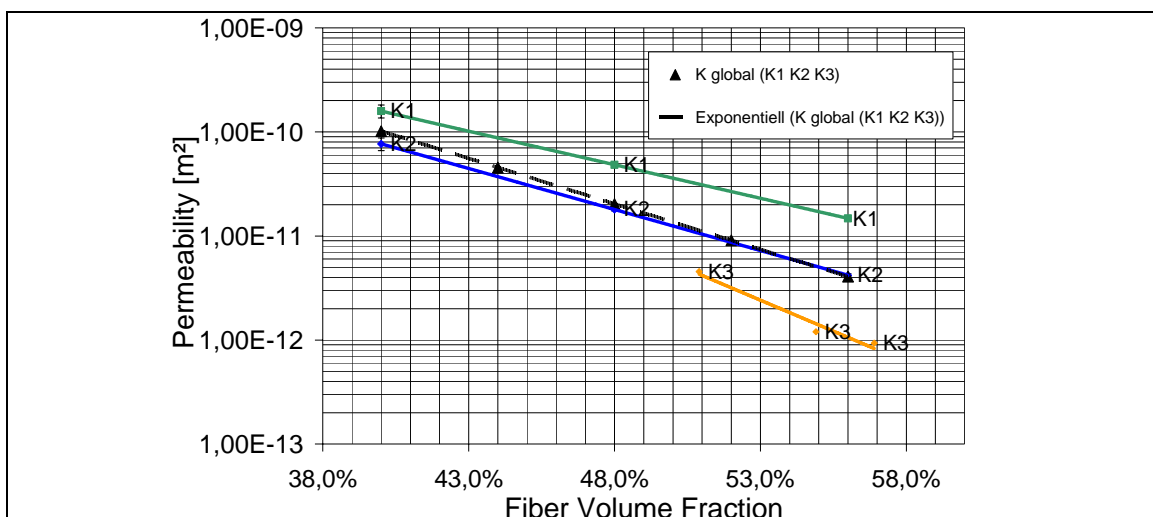

Fig. 1 Permeability values K1, K2 and K3 with exponential regression line.

As a meaningful way to present the results of the pore-size distribution, a cumulative plot that adds up the pore volume fraction from left to right and shows the pore-size diameter has been chosen (fig. 2). This plot allows statements like: For the fiber volume

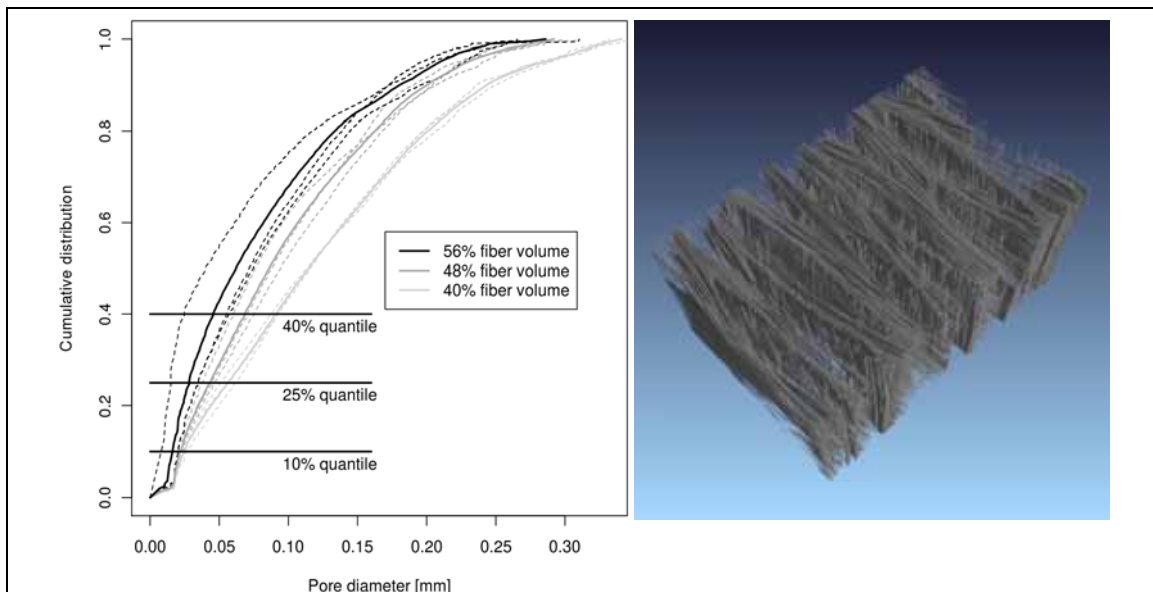fraction of 48 %, 25 % of the overall pore (i.e., matrix) volume consists of pores smaller than 43 µm.

Fig. 2 left: Plot of the cumulative pore volume distribution versus pore diameter, continuous lines are the average, dotted lines are single samples. This plot makes it possible to read out quantiles. right: Image of the analyzed resin structure, the fibers are subtracted of the glass fiber reinforced epoxy image.

To correlate the permeability values with the pore-size distribution, a conversion has to be performed: Bear [11] describes the analogy between the Hagen-Poiseuille equation and Darcy's Law with a 3-directional capillary tube model. Following Hagen-Poiseuille and Darcy, the permeability value K is proportional to the squared diameter ($d^2/96$). In the following table 1, the experimental permeability values are compared with correspondingly computed permeability values determined by the spherical granulometry as described above.

Table 1 Data taken from figures 1 and 2: Fiber volume fractions with corresponding permeability values, calculated flow channel radius and pore-size distribution-quantiles. The directly compared columns are marked in gray.

Fiber volume fraction	Global experimental permeability [m²*10^-11]	10 %-quantile [m*10^-5]	Permeabilitiy calculated with **10 %** quantile pore diameter (d^2/96) [m²*10^-11]	25 %-quantile [m*10^-5]	Permeabilitiy calculated with **25 %** quantile pore diameter (d^2/96) [m²*10^-11]	40 %-quantile [m*10^-5]	Permeabilitiy calculated with **40 %**-quantile pore diameter (d^2/96) [m²*10^-11]
40,0%	10,18	2,55	0,68	5,62	3,30	9,07	8,57
48,0%	2,03	2,20	0,50	4,31	1,94	6,85	4,89
56,0%	0,41	1,71	0,30	2,83	0,84	4,57	2,18

The best fit with experimental data was achieved for cumulative distribution-quantiles of 10, 25 and 40 % for fiber volume fractions of 40, 48 and 56 %, respectively. The choice of the 10 %-quantile as permeability determining quantile at a higher fiber

volume fraction is in accordance with Hazen [11, 12], who as well suggested that smaller particles or pores of a porous structure determine the permeability. The following figure 3 is showing 5 permeability curves. Curve 1-3: determined by the cumulative distribution-quantiles of 10, 25 and 40 %; curve 4 determined by the 40 % cumulative distribution-quantile at a fiber volume fraction of 40 %, the 25 %-quantile at a fiber volume fraction (Vf) of 48 % and the 10 %-quantile at a Vf of 56 % (best fit line); curve 5: the experimentally determined global permeability curve.
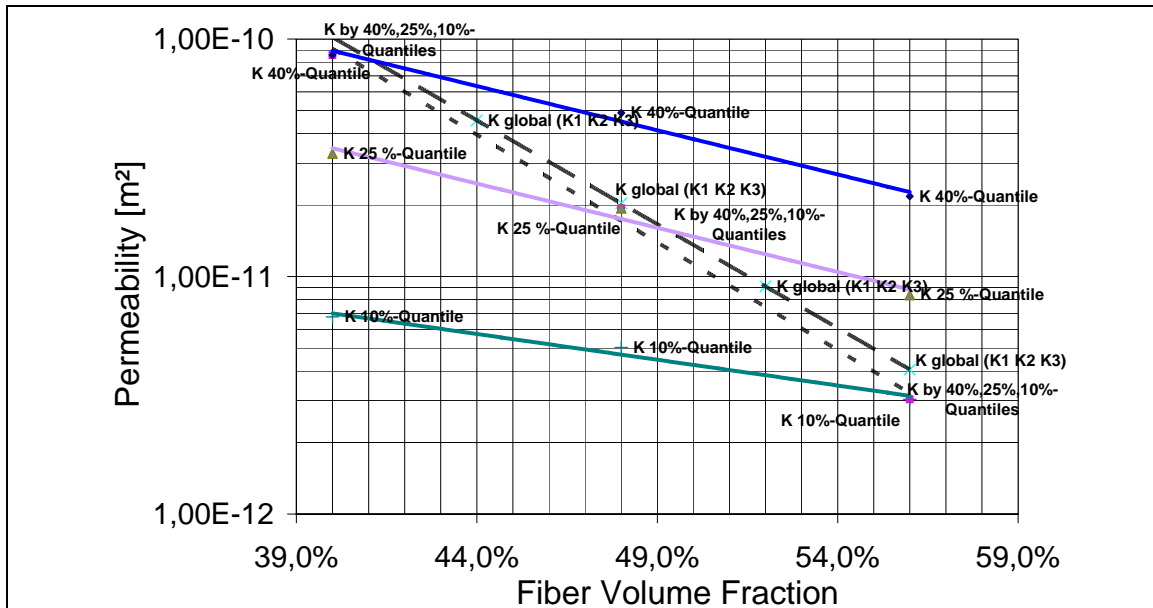

Fig. 3 Plot of the global permeability (as displayed in Figure 1) and the 10 %-, 25 %- and 40 %-quantiles. The dotted line is built up of the following interpolation points: the permeability value calculated from the 40 %-quantile at a Vf of 40%, the permeability value calculated with the 25 %-quantile at a Vf of 48 % and to the permeability at a Vf of 56 % the 10 %-quantile.

CONCLUSION

The study demonstrated the possibility to determine permeability by quantitative analysis of 3D μCT images. Good correlation was achieved with 3 samples used for experimental characterization. Permeability values have been calculated with pore-sizes determined by granulometry measurements. 10 %-, 25 %- and 40 %-quantiles of cumulative pore diameter distributions have been found to be permeability-dominating for fiber volume fractions of 40, 48 and 56 %, respectively. It can be seen in Figure 3 that permeability is overestimated at higher fiber volume fractions if the quantiles from which permeability is calculated is not adjusted to the fiber volume fraction. The applicability of Hagen-Poiseuille for a twill weave textile has been proven. For lower fiber volume fractions, lower cumulative distribution-quantiles are permeability determining. For higher fiber volume fractions, higher cumulative distribution-quantiles are permeability determining. This study has shown the possibility to calculate the permeability by measuring the pore diameters in a laminate. The number of results available is not sufficient to fully validate the 'Cumulative Pore-size Distribution – Permeability' correlation. But it is expected that similar relationships will hold for different kinds of textiles.

ACKNOWLEDGMENT

REFERENCES

1.   Breard, J., Henzel, Y., Trochu, F. and Gauvin, R., "Analysis of Dynamic Flows through Porous Media. Part II: Deformation of a Double-Scale Fibrous Reinforcement", *Polymer Composites*, Vol. 24, No. 3, pages 409-421, (2003).
2.   Elbouazzaoui, O., Drapier, S. and Henrat, P., "An Experimental Assessment of the Saturated Transverse Permeability of Non-Crimped New Concept (NC2) Multiaxial Fabrics", *Journal of Composite Materials*, Vol. 39, No. 13, pages 1169-1193, (2005).
3.   Verleye, B., Morren, G., Lomov, S. V., Sol, H. and Roose, D., "Userfriendly Permeability Predicting Software for Technical Textiles", *5th Industrial Simulation Conference*, (2007).
4.   Dunkers, J. P., Phelan, F. R., Zimba, C. G., Flynn, K. M., Peterson, R. C., Lie, X. D., Fujimoto, J. G. and Parnas, R. S., "Flow Prediction in Real Structures Using Optical Coherence Tomography and Lattice Boltzmann Mathematics", *Proceedings of the Fifth International Conference on Flow Processes in Composite Materials*, (1999).
5.   Gooijer, H., Warmoeskerken, M. M. C. G. and Wassink, J. G., "Flow Resistance of Textile Materials - Part I: Monofilament Fabrics", *Textile Research Journal*, Vol. 73, No. 5, pages 437-443, (2003).
6.   Lomov, S. V., Huysmans, G., Luo, Y., Parnas, R. S., Prodromou, A., Verpoest, I. and Phelan, F. R., "Textile Composites: Modelling Strategies", *Composites Part a-Applied Science and Manufacturing*, Vol. 32, No. 10, pages 1379-1394, (2001).
7.   Nedanov, P. B. and Advani, S. G., "Numerical Computation of the Fiber Preform Permeability Tensor by the Homogenization Method", *Polymer Composites*, Vol. 23, No. 5, pages 758-770, (2002).
8.   Pearce, N. R. L., Guild, F. J. and Summerscales, J., "An Investigation into the Effects of Fabric Architecture on the Processing and Properties of Fibre Reinforced Composites Produced by Resin Transfer Moulding", *Composites Part a-Applied Science and Manufacturing*, Vol. 29, No. 1-2, pages 19-27, (1998).
9.   Ohser, J. and Schladitz, K., "3D Images of Material Structures - Processing and Analysis", *Advances in Statistical Analysis*, Weinheim: Wiley-VCH, (2009).
10.   Redenbach, C., Sarkka, A., Freitag, J. and Schladitz, K., "Anisotropy Analysis of Pressed Point Processes", *Asta-Advances in Statistical Analysis*, Vol. 93, No. 3, pages 237-261, (2009).
11.   Bear, J., "Dynamics of Fluids in Porous Media / Jacob Bear", *Environmental Science Series (New York, 1972-)*, New York: American Elsevier, (1972).
12.   Carrier, W. D., "Goodbye, Hazen; Hello, Kozeny-Carman", *Journal of Geotechnical and Geoenvironmental Engineering*, Vol. 129, No. 11, pages 1054-1056, (2003).
13.   Williams, J. G., Morris, C. E. M. and Ennis, B. C., "Liquid Flow through Aligned Fiber Beds", *Polymer Engineering and Science*, Vol. 14, No. 6, pages 413-419, (1974).
14.   Rieber, G. and Mitschang, P., "2D Permeability Changes Due to Stitching Seams", *Composites Part a-Applied Science and Manufacturing*, Vol. 41, No. 1, pages 2-7, (2010).
15.   Stadtfeld, H. C., Weyrauch, F. and Mitschang, P., "Standardizeable Permeability Work Cell for Fibrous Reinforcements", *FPCM 7 - The 7th International Conference on Flow Processes in Composite Materials*, Delaware, (2004).
16.   Stöven, T., Weyrauch, F., Mitschang, P. and Neitzel, M., "Continuous Monitoring of Three-Dimensional Resin Flow through a Fibre Preform", *Composites Part A - Applied Science and Manufacturing*, Vol. 34, No. 6, pages 475-480, (2003).
17.   Fan, Z. H., Hsiao, K. T. and Advani, S. G., "Experimental Investigation of Dispersion During Flow of Multi-Walled Carbon Nanotube/Polymer Suspension in Fibrous Porous Media", *Carbon*, Vol. 42, No. 4, pages 871-876, (2004).
18.   Matheron, G., "Random Sets and Integral Geometry", *Wiley Series in Probability and Mathematical Statistics*, New York: Wiley, (1974).